ELSEVIER

Chemical Engineering Science 60 (2005) 3587–3598

Chemical Engineering Science

www.elsevier.com/locate/ces

The strength of paraffin gels formed under static and flow conditions

R. Venkatesan[a,1], N.R. Nagarajan[b], K. Paso[a], Y.-B. Yi[c], A.M. Sastry[c], H.S. Fogler[a,*]

[a]*Department of Chemical Engineering, University of Michigan, 2300 Hayward Street Room 3074, Ann Arbor, MI 48109-2136, USA*
[b]*ExxonMobil Upstream Research Company, Houston, TX, USA*
[c]*Department of Mechanical Engineering, University of Michigan, Ann Arbor, MI, USA*

Received 28 October 2004; received in revised form 25 January 2005; accepted 2 February 2005

Abstract

When the temperature of a solution of paraffins in oil is dropped below the 'cloud point' temperature, the high molecular weight *n*-paraffin molecules precipitate out of solution, crystallize and form a gel. The gelation and concomitant deposition of these paraffin gels in crude oil pipelines poses a major transportation problem by reducing the flow efficiency. Implementation of mechanical methods of remediation of paraffin deposition requires knowledge of the gel strength. Rheometric studies were performed on a model system to study the yield strength of paraffin–oil gels formed under various shear and thermal histories. It was observed that when the gel was formed under quiescent (shut-in) conditions, the yield stress of the gel decreased with an increasing cooling rate. However, when a shear stress was exerted on the gel during cooling (as would be experienced in a flow line), the trend of the yield stress vs. cooling rate curve was strongly influenced by the magnitude of this shear stress. Additionally, experimentation over a range of applied shear stresses revealed that the yield stress of the gel reaches a maximum at a moderate value of the applied shear. These rheometric results are explained with the help of 3-D polarized light microscopy observations of the paraffin crystal structure formed under various shear and cooling conditions using static and flow cell systems. The effects of crystal size on the gel properties are enunciated.

Keywords: Microstructure; Non-Newtonian fluids; Paraffin gels; Rheology; Yield stress

1. Introduction

Frost formation (Lee et al., 1997), scale deposition (El-Hattab, 1985), and crystallization fouling of heat exchangers (Bott, 1997) are some examples of solid deposition phenomena that occur in many process systems. Solid deposition typically results in a reduction in the operating efficiency of these systems. Similarly, organic material deposition is a problem encountered in crude oil production and processing operations. Crude oil is a complex mixture containing aromatics, paraffins, naphthenes, asphaltenes, resins, etc. Of these compounds, long-chain paraffins (*n*-alkanes) cause problems because of their tendency to deposit on the cold walls of the sub-sea pipelines. This phenomenon of paraffin deposition is induced because of solubility limits. At reservoir temperatures (in the range of 70–150 °C) and pressures (in the range of 8000–15000 psi), paraffins remain dissolved in the crude oil and the system behaves as a Newtonian liquid. As the crude oil leaves the reservoir and flows through sub-sea pipelines, its temperature drops due to the cold environment of the ocean floor (∼ 4 °C). The solubility of the paraffins in the crude oil decreases drastically with decreasing temperature, hence they precipitate out, crystallize and deposit on the cold pipe walls, thereby restricting flow.

Fig. 1 shows the cross-sectional view of a cut-away segment of a pipeline affected by the paraffin deposition problem. As can be observed, the area available for the crude oil flow has been drastically reduced. Under such circumstances, the part of the pipeline that is plugged would have to be cut out and replaced, resulting in significant operational

* Corresponding author. Tel.: +1 734 763 1361; fax: +1 734 763 0459.
E-mail address: sfogler@umich.edu (H.S. Fogler).
[1] Currently at ChevronTexaco Energy Technology Company, Houston, TX.

0009-2509/$ - see front matter © 2005 Elsevier Ltd. All rights reserved.
doi:10.1016/j.ces.2005.02.045

Fig. 1. Cross-sectional view of a plugged pipeline.

costs. According to the US Department of Energy, remediation of pipeline blockages in water depths of about 400 m can cost $1 million/mile (Anonymous, 2001). In one instance, Lasmo Oil Company (UK) had to abandon an off-shore oil platform due to recurring paraffin plugging problems at a cost of over 100 million dollars. Overall, the paraffin deposition problem is a billion dollar problem in the oil industry.

Paraffins (also interchangeably referred to as 'waxes' here on) start precipitating out of the oil when the solution temperature drops below the 'cloud point' (the wax appearance temperature, 'WAT'). The equilibrium between paraffin (component i) in solution and as a precipitated solid can be determined by equating the fugacities in the liquid and solid phases.

$$x_i \gamma_i^L f_i^{o,L} = s_i \gamma_i^S f_i^{o,S}, \quad (1)$$

where x_i and s_i are the mole fractions of the component i in the liquid and solid phases respectively, γ_i^L and γ_i^S are the activity coefficients in the liquid and solid phases, and f_i^o is the pure component fugacity. Several thermodynamic models have been proposed to describe the equilibrium (Hansen et al., 1988; Coutinho et al., 1995; Lira-Galeana et al., 1996; Coutinho, 1999). The model developed by Coutinho (1999) and modified by Singh et al. (2001a) works very well for describing the thermodynamics of paraffin–oil systems.

The precipitated paraffin molecules crystallize and form a gel at a temperature that is determined by the operating conditions such as the shear rates and cooling rates. Previously, we have been able to correlate this gelation temperature with the shear and thermal histories as well as the composition of the gel (Singh et al., 1999; Venkatesan et al., 2002).

In order to achieve efficient remediation, it is necessary to understand the nature of the wax deposits and study the deposition process. For example, knowledge of the extent of deposition and deposit characteristics will be helpful in choosing the appropriate deposit removal technique and the appropriate way to administer the chosen technique. Two important techniques for removing wax deposits are mechanical pigging and melting the deposit using heat produced by a chemical reaction (Nguyen et al., 2001). Pigging is the standard industrial process of using a 'scraper' device to remove the wax deposits from the pipe walls. If the gel deposit is too hard, then such mechanical methods of remediation would prove to be difficult, as exemplified by instances when the pig has been stuck in the pipeline during the cleaning process. Hence, when the deposit is hard, thermal methods of remediation may be used either to dissolve the wax deposit completely, or to soften the deposit for subsequent pigging. Thus, knowledge of the "hardness" or the strength of the deposit is critical for the successful remediation of the wax deposition problem.

Consequently, the goal of this work was to obtain a thorough understanding of the strength of the wax deposits formed under various conditions. We have previously established that the wax deposit is in the form of a wax–oil gel that hardens with time, i.e., the solid wax content of this gel deposit increases with time; this phenomenon was termed 'aging' of the gel deposit (Singh et al., 2000). We have also observed that the properties of the gel deposit, such as the gelation temperature and the solid wax content, are strong functions not only of the waxy oil composition but also of the shear and thermal histories under which the deposit is formed. Hence, in this work, the gel strength was studied as a function of the mixture composition and the shear and thermal histories during gelation. The results from this work provide valuable information for the operation of oil pipelines.

2. Wax deposition: theory and experiment

In order to obtain insight into the wax deposition phenomenon, a model wax–oil system has been studied using a laboratory flow-loop. The flow-loop simulates the deposition process that occurs in sub-sea pipelines. The setup of the flow-loop and the experimental details are described elsewhere (Singh et al., 2000, 2001b). The flow-loop experiments quantify the growth and aging of the wax–oil gels on the pipe walls. Fig. 2 shows a schematic of the gel deposition process on a cold surface. Many theories, including molecular diffusion, Brownian diffusion, shear dispersion and gravity settling, have been proposed to explain the deposition process (Bern et al., 1980; Burger et al., 1981; Majeed et al., 1990). As discussed in our previous work (Singh et al., 2000), an external convective mass flux of wax molecules from the bulk oil flow towards the cold wall and an internal diffusive flux within the gel layer are responsi-

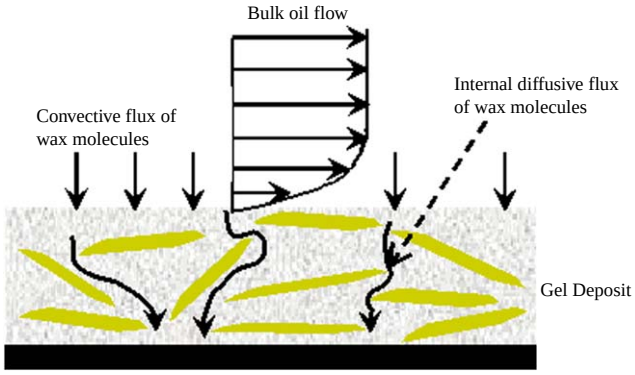

Fig. 2. Schematic of the wax deposition process.

ble for the growth and aging of the gel deposits. Several mathematical models have been proposed to predict the deposition phenomenon based on earlier theories (Bern et al., 1980; Burger et al., 1981; Majeed et al., 1990; Brown et al., 1993; Svendsen, 1993). A mathematical model that predicts both the growth and aging phenomena simultaneously has been developed in our laboratory (Singh et al., 2000). This model is based on heat and mass transfer mechanisms in the bulk flow as well as the internal diffusion mechanism. Fig. 3 shows time trajectories of (a) the ratio of the radius of the pipe available for oil flow to the clean pipe radius and (b) the solid wax content of the deposit. This figure compares typical flow-loop experimental results and the corresponding theoretical predictions. As observed, the model is successful in predicting both the growth and the aging processes of the wax–oil gel deposits in the flow-loop.

As the solid wax content of the gel deposit increases with time due to aging (cf. Fig. 3), the deposit becomes harder—i.e., the gel strength increases with time. Hence, removal of the deposit becomes increasingly difficult with time. As noted earlier, if the strength of the gel deposit becomes too high, then mechanical pigging may not be a viable option. Scheduling pigging operations at a higher frequency is an option. However, due to economic reasons, the pigging frequency is desired to be kept at a minimum. In order to achieve this optimum between pigging frequency and preventing the strength of the gel deposit from reaching high values (as well as keeping the deposit thickness low), it is essential to understand and quantify the effect of the aging process on the gel strength.

3. Yield stress of wax–oil gels

Apart from being crucial in the determination of the pigging schedule, an understanding of the gel strength is also a very important concern in restarting flow in a gelled pipeline. During a temporary shutdown in oil production, due to emergency reasons or otherwise, the waxy crude oil is cooled in the pipelines under quiescent (no flow) conditions. Under such circumstances, the stagnant oil can form a candle of wax–oil gel that blocks the entire pipeline on the ocean floor. In order to restart flow, the gel has to be broken down. This breakage can be achieved by applying pressure on the gel (usually via a liquid at the pipe entrance) until breakdown occurs. In order to predict the breakdown pressure required to restart flow in a safe manner, it is again necessary to estimate the gel strength. The gel strength is measured in terms of the yield stress of the gel. Breakdown of the wax–oil gel occurs if the shear stress exerted on the gel due to the applied pressure exceeds the yield stress of the gel.

Several researchers have investigated models to describe the rheological properties of waxy oils (Davenport and Somper, 1971; Matveenko et al., 1995; Remizov et al., 2000).

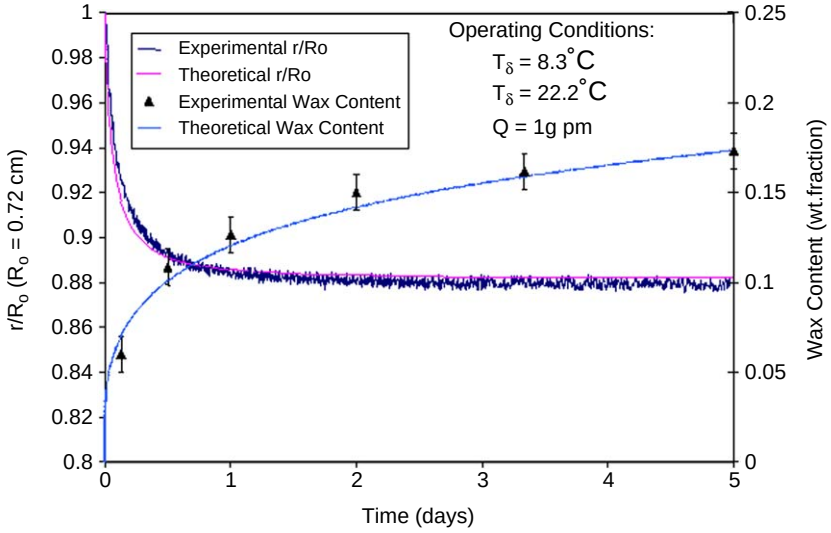

Fig. 3. Comparison between theory and experiment for laminar flow deposition.

They have found that the Casson (1959) model adequately describes the flow characteristics of waxy crudes. The microrheological Casson model describes the stress–strain relationship of a non-Newtonian fluid as:

$$\tau^{1/2} = \tau_y^{1/2} + \eta_C \dot{\gamma}^{1/2} \quad (\text{for } \tau > \tau_y), \tag{2}$$

where τ is the shear stress applied on the fluid, τ_y is the yield stress of the fluid, η_C is the Casson viscosity coefficient and $\dot{\gamma}$ is the resultant strain rate. This model is an improvement on the simple Bingham model for yield stress fluids which describes the stress–strain relationship as

$$\tau = \tau_y + \eta_B \dot{\gamma} \quad (\text{for } \tau > \tau_y), \tag{3}$$

where η_B is the Bingham viscosity coefficient. As noted by Remizov et al. (2000), the Casson model describes the nonlinear plastic flow behavior better than the Bingham model, and may therefore be better suited to describe the rheology of waxy oils.

Several models have also been proposed to describe the breakdown of wax–oil gels (Ananda Rao et al., 1985; Viswanathan and Khilar, 1989; Sestak et al., 1987; Ronningsen, 1992). Typically in these models an empirical structural parameter, defined by the number of 'links' of the solid crystals in the gel structure, is used to describe the breakdown process. The degradation of the wax crystal network is modeled as a decrease in the structural parameter. Once the gel has yielded, these models can describe the subsequent non-Newtonian flow behavior of the waxy oil.

The rheological properties of wax–oil gels depend on the shear and thermal histories to which they are subjected. Clearly, the composition of the gel also affects the gel properties. Gels with higher solid wax content are expected to have a higher yield stress. In general, the following functionality can be written for the yield stress of wax–oil gels:

$$\tau_y = f(\tau_{\text{gel}}, (\mathrm{d}T/\mathrm{d}t), \omega), \tag{4}$$

where τ_y is the yield stress, τ_{gel} is the shear stress applied to the wax–oil mixture during gelation (termed as the 'gelation shear stress' hereafter), $(\mathrm{d}T/\mathrm{d}t)$ is the cooling rate applied during gelation and ω is the solid wax content of the gel. During the deposition of wax–oil gels on the walls of pipelines, the cooling rate is determined by the oil temperature, the wall temperature and the heat transfer properties of the system, whereas the shear stress exerted on the gel deposit is due to the flow of the oil. An equivalent cooling rate for pipe flow can be calculated by equating the wax precipitation rates in the pipe to a quiescent case. An example of such a calculation for the incipient stages of wax deposition can be found in Singh et al. (1999). For the later stages of deposition, an equivalent cooling rate can be determined by calculating the precipitation rates from models, such as one of our previously published deposition models (Singh et al., 2000).

The effect of the cooling rate on the yield stress of wax–oil gels has been studied under static conditions (Ronningsen, 1992; Russell and Chapman, 1971; Cawkwell and Charles, 1989; Chang et al., 2000), however, there has been no comprehensive study of the effect of applying shear during the gelation of waxy oils on the yield stress of the gels formed. Thus, a major goal of this work is to determine, in detail, the effects of the shear and thermal histories as well as the wax content of the gel on the yield stress of the wax–oil gels.

4. Experimental

4.1. Materials

In this work, a model wax–oil system has been used to form the wax–oil gels. The oil used was Coray-15$^{\text{TM}}$, a lubricating mineral oil (product of Exxon), while the wax was paraffinic wax with a carbon number distribution of C22 to C39, as shown in Fig. 4. Fig. 5 shows the cloud point curve (solubility curve) of the paraffin wax in the model oil. A mixture of 5% (by weight) wax in oil was used for all experiments, except where stated otherwise. The cloud point of the 5% wax in oil mixture was 83 °F (28.3 °C).

4.2. Rheometric studies

To study the yield stress of the wax–oil gels, a controlled stress rheometer—universal stress rheometer SR5 from Rheometric Scientific Inc. was used. This rheometer has temperature control using a Peltier plate device, which is essential for controlling the thermal history of the sample accurately. A cone-and-plate geometry (cone dimensions: 40 mm diameter and 2° cone angle) was used for all the experiments.

4.3. Microscope studies

A cross-polarized light microscope (Nikon Eclipse E600) was used to study the crystal structure of the wax–oil gel formed at quiescent conditions. A "z-drive" was used for three-dimensional imaging of the gel structure. A Bionomic cooling system (from 20-20 Technology Inc.) was mounted onto the microscope for controlling the temperature and the cooling rate, and an aluminum/sapphire slide was used for good thermal conductivity. The images were captured using an ORCA-ER digital camera (from Hamamatsu) connected to the microscope.

4.4. Flow-cell microscopy studies

A Cambridge Optical Shearing System (CSS 450) from Linkam Scientific Instruments Co was used to observe the crystal structure of the paraffin–oil gels formed under shear. The system was mounted onto a microscope and the evolution of the crystal structure was captured using a video camera.

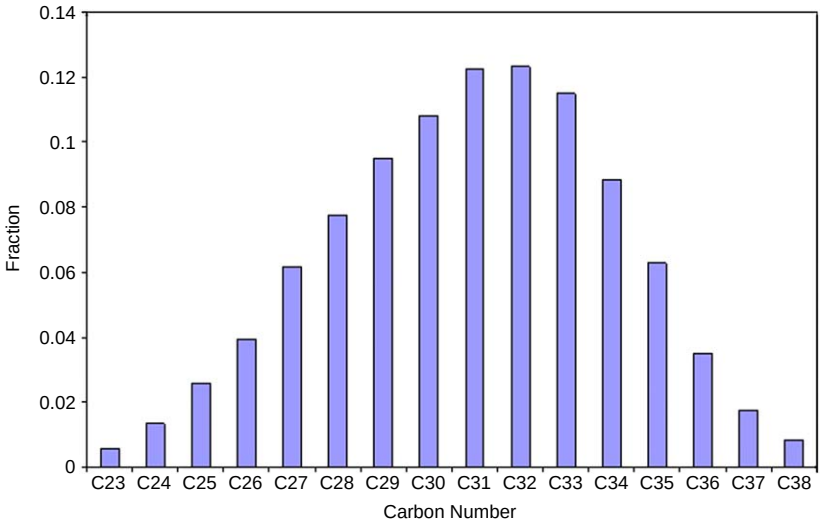

Fig. 4. Carbon number distribution of the paraffin wax.

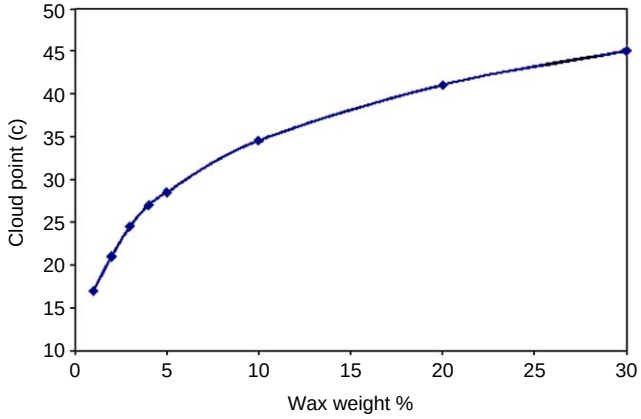

Fig. 5. Cloud point curve for paraffin wax in Coray-15.

4.5. Yield stress measurements

The effect of the solid wax content on the yield stress of wax–oil gels was studied by using samples prepared with various amounts of wax. For studying the effect of the shear and thermal histories, a fixed wax content of 5% (ratio by weight in the oil) was used. The mixture was initially heated up to 120 °F and then cooled down to 40 °F in the rheometer under various cooling rates and applied stresses. At the final temperature of 40 °F, the mixture had gelled and the applied stress did not result in any movement of the gel at this point ($\dot{\gamma} = 0$). The gel was then held at 40 °F and a shear stress was exerted. The shear stress was ramped up at a rate of 20 Pa/min, until the sample yielded. The yield stress was defined as the point where there was a significant increase in the strain and a concomitant decrease in the viscosity. One of the potential problems while testing for the yield stress using a rheometer is the possibility of slip at the surfaces. Magnin and Piau (1990) used strain field observations to study the effect of slip on the measurement of yield stress of an aqueous gel, and found that slip played an important role when using smooth surfaces. When the surfaces roughness was sufficiently high ($> 250\,\mu$m), slip was found to be negligible. Patton and Casad (1970) performed cold spot testing on model wax–oil systems and found that failure was cohesive (yielding) when using roughened surfaces. They also observed that there was no correlation between the amount of deposit and the surface roughness. In our present work, the surfaces of the rheometer were sufficiently rough so that no slip was observed under the test conditions reported here. Visual observation was used to determine whether slip occurred. Further, after apparent yielding of the gel, the rheometer surfaces were separated to observe the failure mode. For example, if the failure was due to slip, then the slip surface would be practically clean and the gel would be almost intact. Slip, or adhesive failure at the surface, became a problem only when testing with samples whose yield stresses were higher than those of the samples used in this work. Wardhaugh and Boger (1991) tested the yield stress of waxy crudes and observed that the yielding behavior was consistent with the fracture of solids. Chang et al. (1998) have described the yielding behavior of a waxy crude oil as having three distinct characteristics—an elastic response, a creep and a fracture. The shear stress at the point of fracture is the value of practical importance and is usually taken as the yield stress. This definition of yield stress has been used in our work as well. Fig. 6 shows typical rheometric responses when determining the yield stress. Initially, at low values of the applied shear stress ($< \tau_y$), the rheometer cannot determine the viscosity in as much as no sample movement can be recorded. When the shear stress reaches close to the yield value, a creep response is observed and, at about 190 Pa for one sample and 850 Pa for another, the point of fracture is reached and is manifested in the form of a sudden decrease in the viscosity. Thus, the yield stress is

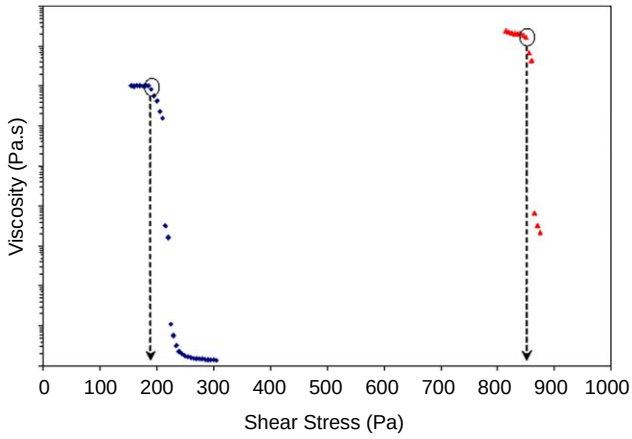

Fig. 6. Transient plot of typical rheological experiments.

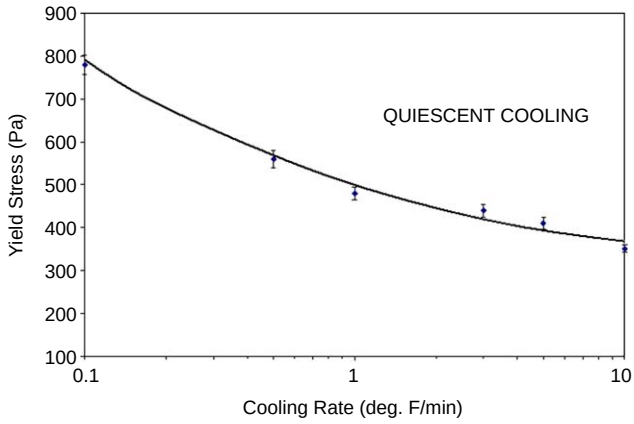

Fig. 7. Decrease in the yield stress with an increasing cooling rate ($\tau_{gel} = 0$).

taken as 190 and 850 Pa, respectively, in the two cases. These experimental results were reproducible within 10–15%.

5. Results and discussions

5.1. Variation of yield stress with cooling rate

5.1.1. Cooling under quiescent conditions

First, the effect of cooling rate on the yield stress was studied by cooling a sample of the wax–oil mixture under quiescent conditions—i.e., the sample was not subjected to any shear stress while cooling. In pipelines, this situation occurs before a restart, when the crude oil is cooled under shutdown (stagnant) conditions. The yield stress of the wax–oil gel was studied as a function of the cooling rate. While varying the cooling rate, it was noted that the kinetics of paraffin precipitation could affect the yield stress measurement if the cooling rate were too high. Clearly, if the cooling rate is much higher than the rate of precipitation, the wax–oil solution will be highly super-saturated at any given temperature. Thus, the waxes will continue to precipitate even after the final temperature (40 °F) has been reached, and the yield stress measured will vary with the time spent at the final temperature. Therefore, it was necessary to maintain the cooling rates within the "equilibrium cooling rate" regime so that the precipitation kinetics do not affect the value of the yield stress. For the system studied, this equilibrium cooling regime was determined by studying the effect of the "holding time" on the measured value of the yield stress. The holding time is the time that the sample was held quiescently at 40 °F before the stress ramp was applied. The holding time was varied from 1 min to 1 h. If the value of the yield stress measured subsequently did not vary with the holding time (within experimental error), then the cooling rate was classified as being within the equilibrium cooling rate regime. The equilibrium cooling rate regime was thus determined to extend up to a cooling rate of about 10 °F/min. At higher cooling rates, the yield stress varied with the holding time. Thus, the highest cooling rate used in this study was 10 °F/min. This equilibrium cooling rate regime can also be determined by observing the apparent cloud point temperature at various cooling rates; similar results were observed using this method.

The effect of the cooling rate on the strength of crude oil gels formed under static conditions has been previously studied (Ronningsen, 1992; Russell and Chapman, 1971; Cawkwell and Charles, 1989; Chang et al., 2000), but these literature results are not in agreement. For example, Russell and Chapman (1971) and Cawkwell and Charles (1989) observed that rapid cooling produced stronger gels, whereas Ronningsen (1992) and Chang et al. (2000) observed that slower cooling rates resulted in stronger gels. The results of our current work are shown in Fig. 7. The yield stress was observed to decrease with an increasing cooling rate. Thus, our results are in agreement with the results of Ronningsen and Chang et al. It may be noted that the presence of other components and impurities, such as asphaltenes and inorganic material, in crude oil could perhaps lead to results such as observed by Russell and Chapman, and by Cawkwell and Charles. Results qualitatively similar to ours have been also reported by Albano et al. (in press), although for a different system. Albano et al. observed that the shear strength of a model metallic glass, formed by cooling the precursor liquid, critically depended on the thermal history of the precursor liquid. The glass produced by quenching the liquid from a higher temperature had lower shear strength than the glass produced by quenching the liquid from a lower temperature.

The explanation for the observed decrease in the yield stress with an increasing cooling rate can be explained by considering the time available for the growth of the wax crystal network. Given the same upper and lower temperature limits (120–40 °F), a lower cooling rate provides more time for crystal growth, resulting in the formation of larger crystals. On the other hand, under a higher cooling rate, the rate of precipitation is faster and there is not as much time for crystal growth—resulting in smaller crystals. Bakin et al.

(1994) have stated and experimentally verified an equation relating the maximum size of crystallites formed during the crystallization of segregating metallic solid solutions to the cooling rate. According to this equation,

$$L_{\max} \propto (\mathrm{d}T/\mathrm{d}t)^{-0.5}, \quad (5)$$

where $L_{\max}$ is the maximum crystal length in the system and $(\mathrm{d}T/\mathrm{d}t)$ is the cooling rate. This equation is valid as long as there are no temperature gradients within the system. As will be explained below, the formation of longer crystals will result in a stronger gel network. Hence, a lower cooling rate results in the formation of stronger gels. In order to examine such a crystal size behavior for the wax–oil system, microscopic observations were made on wax–oil gels formed at various cooling rates.

5.1.1.1. Microscopic observations of wax structure. A 5% wax-in-oil mixture was heated above its cloud point, placed under a cross-polarized microscope and cooled at a specified rate by a Bionomic cooling system. The cooling rate was varied to study its effect on the structure of the wax network formed.

Fig. 8 shows the images of wax–oil samples cooled down to the same temperature at two different cooling rates. The wax particles formed under the lower cooling rate (1.8 °F/min) are observed to be larger than those formed at the higher cooling rate (10.8 °F/min). The maximum length of wax crystals formed at 1.8 °F/min was about 37 μm and the maximum crystal size at 10 °F/min was about 17 μm. Thus, the ratio of the maximum crystal lengths is $R_{L_{\max}} = 37/17 = 2.2$, whereas the ratio of the inverse square roots of the cooling rates is $R_{CR} = (1.8/10.8)^{-0.5} = 2.45$. Hence, the maximum crystal length scales with the cooling rate close to the prediction of Eq. (5) ($R_{L_{\max}} \approx R_{CR}$). It was also observed (cf. Fig. 8) that more wax crystals were formed at the higher cooling rate. That is, the crystal size decreased and the crystal number density increased with an increasing cooling rate. Under conditions of equilibrium cooling, the total amount of precipitated wax is the same at a given temperature regardless of the cooling rate. Thus, the formation of a greater number of solid wax particles implies smaller particle size.

In order to quantify the dimensions better, 3-D imaging of the gel was undertaken. Since the gel formed on the slide has a finite thickness, several 2-D images such as the ones shown in Fig. 8 can be captured at various planes along the z-axis. A "z-drive" was used for this purpose. The stack of 2-D images was then converted to a 3-D image using an image processing software. Fig. 9 shows the image of the wax crystal network formed under the higher cooling rate (10.8 °F/min). The projection of the 3-D image rotated by an angle of 30° about the horizontal axis (x-axis) is shown at the top, whereas the projection of the 3-D image rotated by an angle of 30° about the vertical axis (y-axis) is shown at the bottom. Note that the image shown in Fig. 8 (bottom) is the projection of the same 3-D object in the x–y plane without any rotation. The animated 3-D image revealed that the crystals were thin platelets.

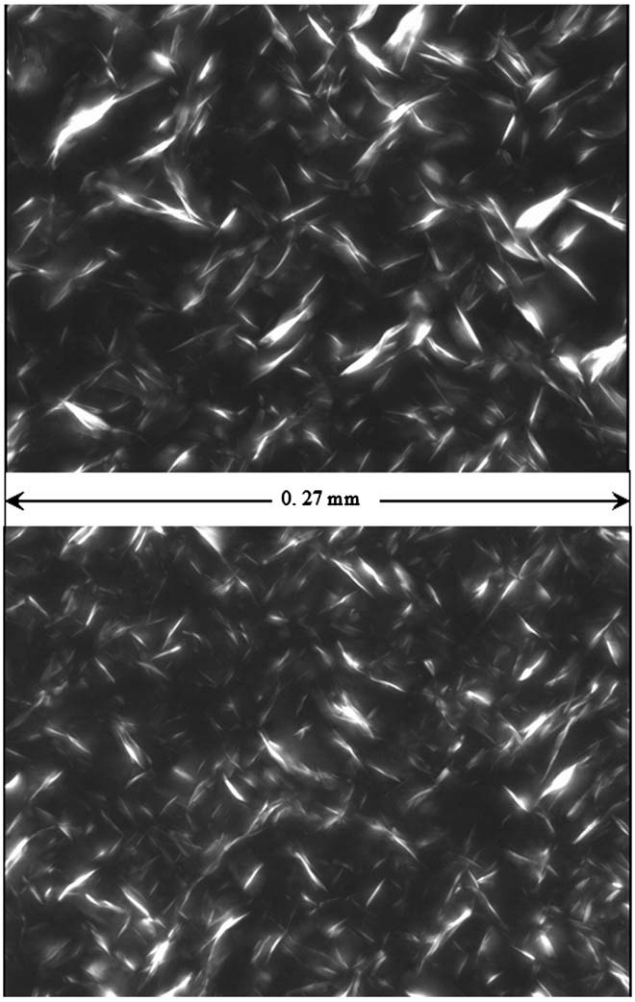

Fig. 8. The effect of cooling rate on the size and number of wax crystals (Top: 1.8 °F/min; Bottom: 10.8 °F/min): A lower cooling rate results in bigger and lower number of crystals.

The wax crystals formed within a volume of $1.77 * 10^{-3}\,\mathrm{mm}^3$ were observed. At the lower cooling rate (1.8 °F/min), about 250 particles were formed in this volume. The approximate median dimensions of the particles were: 19.1 μm length, 15.0 μm width and 1.0 μm thickness. At the higher cooling rate, about 480 particles were observed within this same volume. The median dimensions in this case were: 12.2 μm length, 12.0 μm width and 1.0 μm thickness. The thickness of the platelets appears to be the same in either case, indicating that the crystal growth is two-dimensional.

As will be explained later, the larger particles result in a stronger gel. Hence, the strength of the gel formed at a lower cooling rate is higher. This effect of the crystal size also plays an important role in the action of commercial 'pour point' depressant chemicals. These chemicals prevent the aggregation of wax crystals, thus resulting in

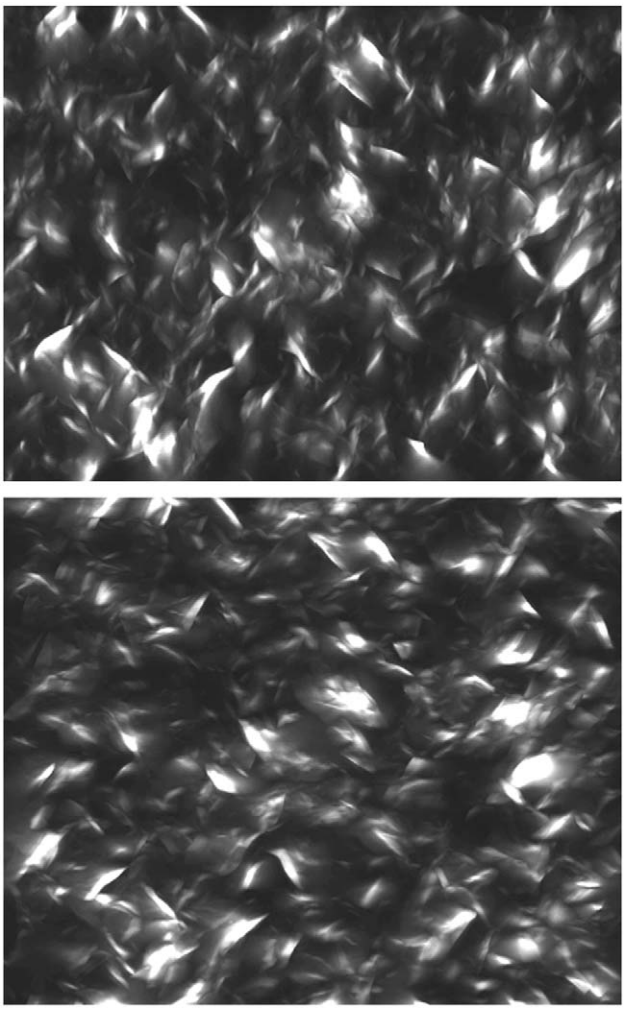

Fig. 9. Projections of the 3-D image rotated by an angle of 30° about the x-axis (top) and about the y-axis (bottom).

smaller platelets and lower pour point temperatures and gel strength. We have also observed this effect when adding asphaltenes (a polar fraction of crude oil) to wax–oil mixtures: the addition of asphaltenes reduces the gelation temperature and gel strength by leading to the formation of smaller crystals.

5.1.2. Cooling under an applied shear stress

The next set of experiments focused on cooling a wax–oil sample under the influence of a shear stress. This situation is analogous to the formation of gel deposits in oil pipelines under flow conditions. A shear stress of 5 Pa was used, and various cooling rates were studied. In a pipeline, a shear stress of 5 Pa would be exerted on the incipient gel deposit by an oil flow rate of approximately 16,000 barrels oil per day in a 10-in pipeline with an oil viscosity of 10 cp (mPa s).

Fig. 10 shows the variation of the yield stress with cooling rate, when the gelation occurred under a shear stress of 5 Pa. This behavior was exactly the opposite to the behavior of the gels formed under no shear. The yield stress, in this

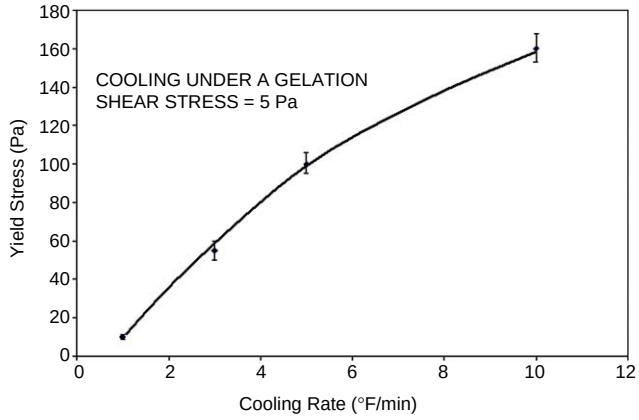

Fig. 10. Increase in the yield stress with an increasing cooling rate ($\tau_{gel} = 5$ Pa).

case, increased with an increasing cooling rate. This behavior can be explained by considering the effect of the applied shear stress (the gelation shear stress, τ_{gel}) on the formation of the crystal network during the cooling process. The gelation shear stress tends to break up the crystal network even as it forms. A lower cooling rate implies that the wax–oil mixture is subjected to the shear stress for a longer time before the sample completely gels. A wax–oil mixture that has been subjected to the gelation stress for a longer time is likely to result in a crystal network that is degraded to a greater extent. Hence, the gel formed under shear at a lower cooling rate is weaker. At a higher cooling rate, the precipitation rate is faster, and the gelation occurs sooner. Hence, in this case, the wax–oil mixture is under the gelation shear stress for a shorter duration. Therefore, the network is degraded to a lower extent, resulting in a stronger gel. It was previously observed in our lab that the gelation temperature increased with an increasing cooling rate when the gelation occurred under an applied shear stress (Singh et al., 1999). That observation correlates well with the current observation of an increase in the yield stress with an increasing cooling rate. Evidence for the breakdown of the network was observed using flow cell microscopy and is described in the next section.

5.2. Variation of yield stress with gelation shear stress

To summarize the previous results, it has been observed that the yield stress of the wax–oil gel decreases with an increasing cooling rate when cooled under quiescent conditions, but increases with an increasing cooling rate when cooled under a gelation shear stress of $\tau_{gel} = 5$ Pa. Thus the magnitude of the shear stress applied during gelation determines the effect of cooling rate on the yield stress. To elucidate the effect of this gelation shear stress in greater detail, the yield stress of wax–oil gels formed under various gelation shear stresses, but under the same cooling rate, was studied.

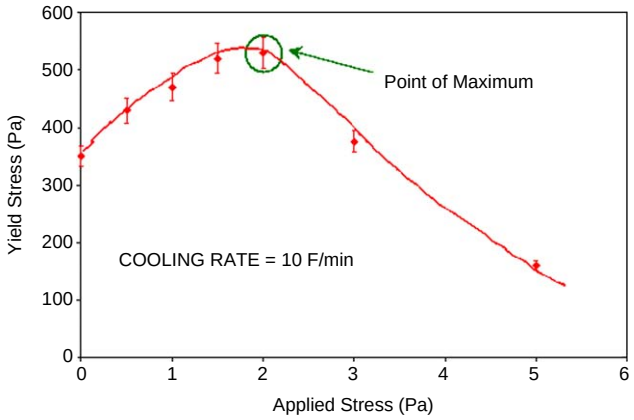

Fig. 11. Variation of yield stress with the gelation shear stress: The existence of a peak.

Fig. 11 shows the variation of the yield stress with the gelation shear stress. The cooling rate was fixed at 10 °F/min and the gelation shear stress was varied (from $\tau_{gel} = 0$–5 Pa). At low values of gelation shear stress (< 2 Pa), the yield stress increased with an increasing gelation stress. A maximum in the yield stress was observed at a gelation stress of 2 Pa. Thereafter, the yield stress decreased with an increasing gelation stress. The maximum in the yield stress is due to the differences in the wax crystal structure formed under various shear stresses. In order to visually observe the effect of gelation shear on the formation of wax crystal network, the gelation process was studied under various shear rates using a Linkam flow cell coupled with a microscope.

5.2.1. Flow cell observations of wax network

Fig. 12 shows the wax crystal network formed under various shear rates. Due to limitations of the flow cell, a controlled shear stress could not be imposed; thus a controlled shear rate was imposed instead. Under each of the three shear rates, 41 images were subsequently taken from the sample at evenly-spaced depths 1 μm apart, for analysis of the geometrical properties of the 3-D wax crystal structure and their correlations to shear rate. The uniformity of distributions of objects in each cross-sectional view, independent of depth, suggests that each gel crystal is roughly "penny-shaped," i.e., a thin platelet having, generally, an elliptical cross-section. Alternatively, they could be characterized as oblate spheroids (resulting in the elliptical cross-section), although the resolution obtained in imaging is probably not sufficient to convincingly discern slight differences in aspect ratio which would point to one characterization or another. In this study, an elliptical cross-sectioned cylinder (thin platelet) was assumed as the shape of each individual wax crystal due to the difficulty in determination of crystal extension in the depth dimension. The ellipse's aspect ratio is defined hereafter as the ratio of major/minor axis. The image thresholds were determined in such a way that the overall volume fractions of the structure estimated from the

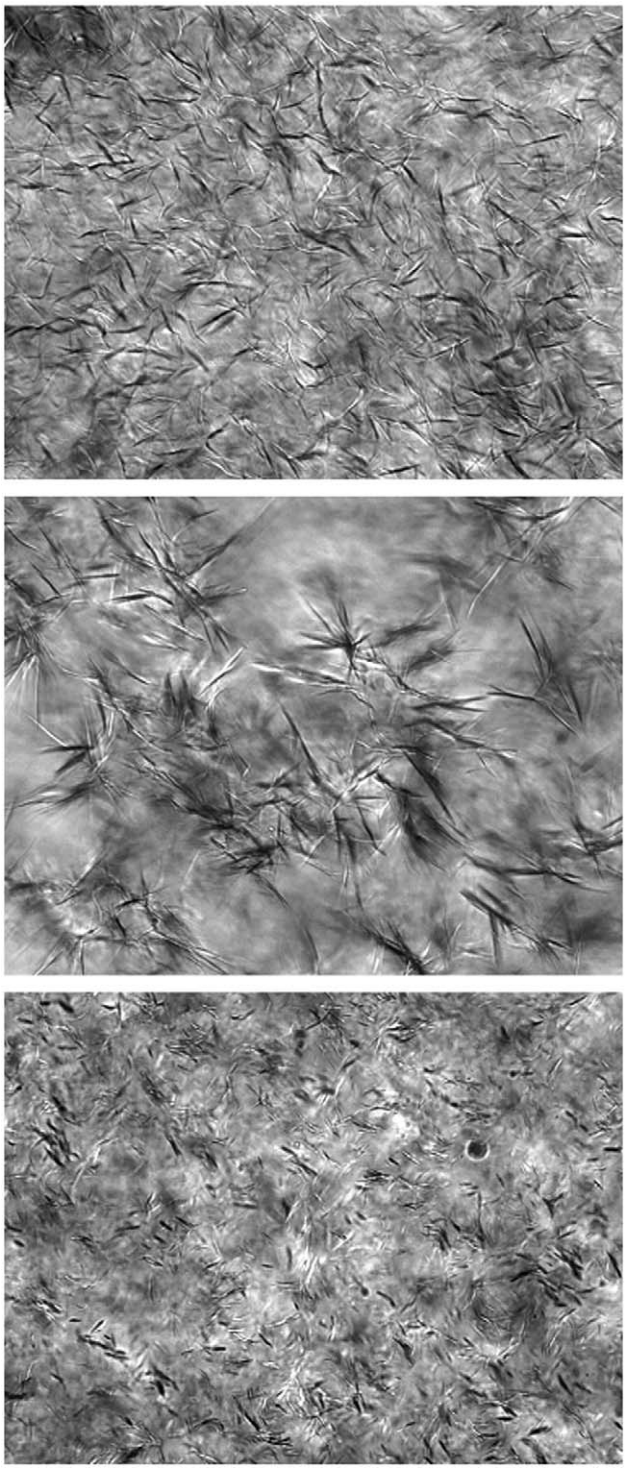

Fig. 12. Wax crystal structure formed under shear (all figures have same scale). Top: No shear conditions (quiescent); Middle: Low shear conditions ($\dot{\gamma} = 0.1$ rad/s) and Bottom: High shear conditions ($\dot{\gamma} = 1$ rad/s).

grayscale images were approximately 3%, which is known from the experiments and invariable under different shear rates.

Previous studies on clustering and percolation problems of randomized particulate systems showed that at low

volume fraction, the cluster statistics are extremely sensitive to the aspect ratio of individual particles (Yi and Sastry, 2002). Specifically, particles of large aspect ratios tend to be highly correlated and large clusters arise. For example, at a volume fraction of 3%, the cluster number of four particles in a system of ellipsoids of aspect ratio 10 could be 10 times that of a system of spheres (aspect ratio = 1), requiring a higher stress to break down the interconnected network. Therefore, higher aspect ratio is related to higher degree of entanglements, which leads to stronger crystal structures and higher yield stresses. On the other hand, the areal fractions/volume fractions measured from the image analyses were below those of percolated arrays of both ellipses in 2-D or ellipsoids in 3-D. For materials containing particles below the percolation point, surface area is critical, since the internal load is borne by stress transfer between the amorphous phase and surface forces on the paraffin crystals. At the same volume fraction, smaller crystal particles have larger total surface area, making it easier to transfer load internally among particles. As a result, smaller crystal size results in more flexible structures and smaller yield stresses.

Fig. 12(a) shows the wax crystals formed under quiescent conditions ($\dot{\gamma} = 0$). 2-D images using a phase contrast microscope are shown in this figure; hence, the wax crystals are seen as black in this case. The analyzed crystal platelets have mean length 6.58 μm, width 2.26 μm, and aspect ratio 3.13, averaged over a total number of 44 detected objects. Matlab© image processing toolbox was used in the object detections and feature extractions. When a moderate gelation shear rate is applied ($\dot{\gamma} = 0.1$ rad/s), larger wax crystals (platelets) are formed as shown in Fig. 12(b). The analyzed platelets have mean length 8.36 μm, width 2.15 μm and aspect ratio 4.02, averaged over a total number of 38 detected objects. The shear applied during the formation of the crystals leads to aggregation of the wax crystals, resulting in larger crystals. As noted earlier, the larger crystals result in a stronger network. Further, the shear results in a larger aspect ratio and a greater degree of entanglements between the wax platelets as observed from Fig. 12(b). Hence, the yield stress of gels formed under a moderate value of the gelation stress is higher than that of gels formed under quiescent conditions. On the other hand, when the gelation shear rate is increased to a high value ($\dot{\gamma} = 1$ rad/s), it breaks down the crystal network. Fig. 12(c) shows that the high shear rate imposed during crystal formation results in the formation of smaller crystals (mean length and width are 5.18 and 1.85 μm, respectively, averaged over 77 detected objects) with lower aspect ratios (2.94). Hence, the yield stress decreases with increasing gelation stress at higher values of gelation stress.

Thus, the presence of gelation shear stress is seen to result in two competing effects: the tendency to aggregate the precipitating crystals and the tendency to break down the growing crystals. As the gelation shear stress increases, the breakdown tendency increases. Hence, the maximum yield stress occurs when the gelation stress is just enough to achieve maximum size of crystals, without being high enough to break down the structure.

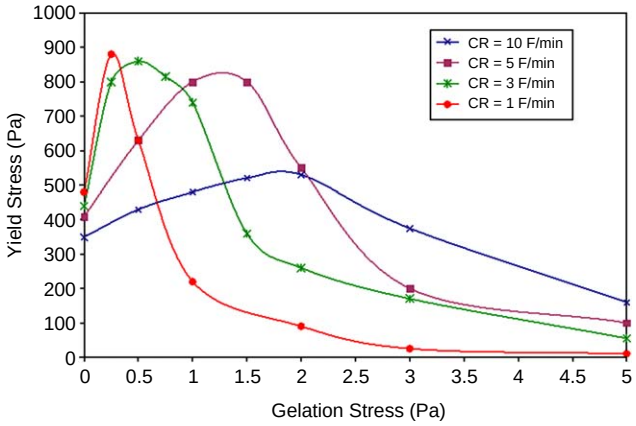

Fig. 13. The overall behavior of the yield stress: The interplay between the shear and thermal histories.

5.3. The interacting effects of the shear and thermal histories

Fig. 13 shows the dependence of the yield stress on gelation stress for various values of cooling rate. For every cooling rate used, the yield stress showed a maximum when plotted as a function of the gelation shear stress. This peak (maximum) value of the yield stress was higher at a lower cooling rate. Also, this maximum did not occur at the same value of the gelation stress for all the cooling rates studied. At a higher cooling rate, this maximum in the yield stress occurred at a higher value of the gelation stress. The shift to a higher value of τ_{gel} shows the interacting effects of the shear and thermal histories, i.e., the gelation stress and cooling rate. At a higher cooling rate, the rate of wax precipitation is higher. Hence, a higher stress is necessary either to aggregate the crystals, or to break down the structure. Thus, a higher gelation stress is necessary to achieve the maximum in the yield stress—hence the shift. This is also the reason for the progressive widening of the peak with an increasing cooling rate.

5.4. Variation of yield stress with wax content

The results described thus far have been obtained with a fixed wax content (5 weight %) in the mineral oil. During the wax deposition process in pipelines, the gel deposit ages with time due to the internal diffusion of wax molecules within the gel. Thus the solid wax content of the gel increases with time. An increasing solid wax fraction in the gel is expected to result in an increasing yield stress of the gel. Rheometric experiments were performed to quantify the effect of wax content on the yield stress of the gel. Wax–oil mixtures with various wax contents were cooled down under identical conditions to 40 °F. Fig. 14 is a plot of the gel

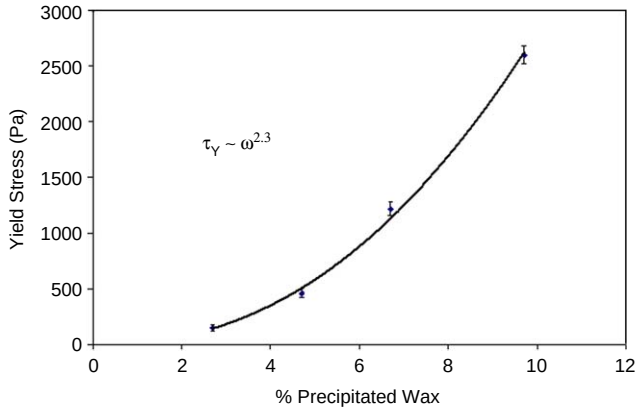

Fig. 14. Variation of yield stress with the solid wax content.

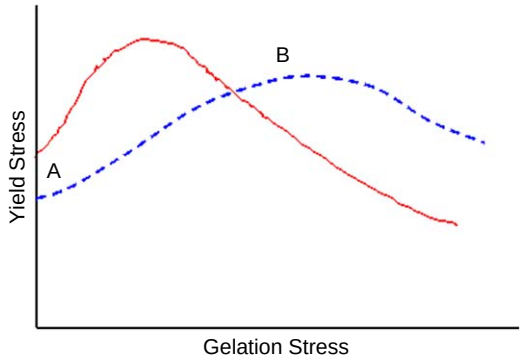

Fig. 15. Schematic of Fig. 13 showing yield stress behavior for two cooling rates.

yield stress as a function of the amount of wax precipitated at 40 °F (the solid wax content of the gel). Clearly, a gel with a higher solid wax content exhibits a higher yield stress. The yield stress, τ_y, can be related to the solid wax content of the gel, ω, as

$$\tau_y \propto \omega^n. \tag{6}$$

For colloidal systems, the equation relating the yield stress to the solid fraction is known to follow such an exponential form. From Fig. 14, the value of the exponent n for the wax–oil system is correlated to be about 2.3.

It may be noted that the wax contents studied here are in the typical range when considering the restart issue in crude oil pipelines (except for consideration of very high wax content crudes). This is because aging, in general, is not a critical factor under shut- in conditions. When considering deposits formed under flow, the aging process is likely to result in wax contents higher than those studied in this work. However, due to equipment limitations, it was impractical to study much higher wax contents.

5.5. Oilfield implications

The results of the rheometric studies have some key implications for field operations of crude oil pipelines. Fig. 15 is a schematic of Fig. 13 and is shown to demonstrate the concepts discussed in this section. Fig. 15 shows the relationship between τ_y and τ_{gel} for two different cooling rates A and B. An obvious connotation of this work is to identify and avoid the "peak zone" in the yield stress (cf. Figs. 13 and 15). The peak zone will be different for different crude oils, so rheometric tests have to be performed for each crude oil to identify the peak zone. By varying the cooling rate or the shear stress (within operational limits), the strength of the gels formed can be varied. The lower the gel strength, the easier is the removal process.

When the crude oil flow in a pipeline has to be stopped for any reason, it is sometimes the industrial practice to let the oil circulate via a small loop. This re-circulation is performed in order to avoid oil stagnation, so that the extent of gel formation may be reduced. A low re-circulating flow rate exerts a small shear stress on the gel while it is being formed. As we have shown before, a small applied shear stress may result in deposits that are harder than those formed under quiescent conditions. The re-circulation flow rate would change the cooling rate as compared to the quiescent case. Fig. 15 compares the two cases. The point "A" in Fig. 15 shows the quiescent case. Re-circulation can shift the operating point to point "B". Thus, the effect of the shear stress induced by the flow may result in an increase in the resultant gel strength. Thus, re-circulation can lead to the formation of deposits that are harder to remove. Hence, the flow rate for the circulation has to be maintained such that the yield stress of the deposit formed is not higher (preferably lower) than the stagnant deposit.

6. Summary

The yield stress of a wax–oil gel is a complex function of the gel composition and shear and thermal histories under which the gel has been formed. The wax crystals are observed to form platelet structures that grow in two dimensions. When the gel is formed under quiescent cooling, the yield stress decreases with an increasing cooling rate. The wax crystal network formed at a lower cooling rate is stronger due to the formation of larger wax crystal platelets. However, when the gel is formed under a high gelation stress, the yield stress of the gel increases with an increasing cooling rate. Experimentation with a range of gelation shear stresses has revealed that, at a fixed cooling rate, the yield stress reaches a maximum at a moderate value of the gelation shear stress. The initial increase in the yield stress with respect to gelation stress is found to be a result of the aggregation and entanglements of solid wax crystal platelets induced by the shear. The subsequent decrease in the yield stress at high values of the gelation stress is because of the breakdown of the wax network by the shear. These results are shown to have a direct bearing on the operation of crude oil pipelines.

Acknowledgments

We thank Professor Ron Larson (Chemical Engineering department, University of Michigan) for allowing use of the Linkam flow cell. We also thank the management of ExxonMobil Upstream Research Company for permission to publish part of the data shown in the paper and the URC technical staff—especially Alan Stone—for their help in the laboratory.

References

Albano, F., Lacevic, N., Falk, M.L., Glotzer, S.C., 2004. Materials Science & Engineering A 375–377, 671–674.
Ananda Rao, B.M., Mahajan, S.P., Khilar, K.C., 1985. Canadian Journal of Chemical Engineering 63, 170–172.
Anonymous, 2001. Oil & Gas Journal 99, 56.
Bakin, A.S., Romanenko, V.N., Schilz, J., Nikitina, G.V., Ivanov, D.I., 1994. Scripta Metallurgica et Materialia 31, 1131–1134.
Bern, P.A., Withers, V.R., Cairns, R.J.R., 1980. Proceedings of the European Offshore Petroleum Conference Exhibition, vol. 206, pp. 571–578.
Bott, T.R., 1997. Experimental Thermal and Fluid Science 14, 356–360.
Brown, T.S., Niesen, V.G., Erickson, D.D., 1993. Production Operations and Engineering Proceedings SPE Annual Technical Conference and Exhibition, pp. 353–368.
Burger, E.D., Perkins, T.K., Striegler, J.H., 1981. Journal of Petroleum Technology 33, 1075–1086.
Casson, N., 1959. In: Mill, C.C. (Ed.), Rheology of Disperse Systems. Pergamon, New York, pp. 84–104.
Cawkwell, M.G., Charles, M.E., 1989. Journal of Pipelines 7, 251–264.
Chang, C., Boger, D.V., Nguyen, Q.D., 1998. Industrial & Engineering Chemistry Research 37, 1551–1559.
Chang, C., Boger, D.V., Nguyen, Q.D., 2000. SPE Journal 5, 148–157.
Coutinho, J.A.P., 1999. Fluid Phase Equilibria 158–160.
Coutinho, J.A.P., Andersen, S.I., Stenby, E.H., 1995. Fluid Phase Equilibria 103, 23–39.
Davenport, T.C., Somper, R.S.H., 1971. Journal of the Institute of Petroleum 55, 86–105.
El-Hattab, M.I., 1985. Journal of Petroleum Technology 37, 1640–1652.
Hansen, J.H., Fredenslund, A., Pedersen, K.S., Ronningsen, H.P., 1988. A.I.Ch.E. Journal 34, 1937–1942.
Lee, K.-S., Kim, W.-S., Lee, T.-H., 1997. International Journal of Heat and Mass Transfer 40, 4359–4365.
Lira-Galeana, C., Firoozabadi, A., Prausnitz, J.M., 1996. A.I.Ch.E. Journal 42, 239–248.
Magnin, A., Piau, J.M., 1990. Journal of Non-Newtonian Fluid Mechanics 36, 85–108.
Majeed, A., Bringedal, B., Overa, S., 1990. Oil & Gas Journal 88, 63–69.
Matveenko, V.N., Kirsanov, E.A., Remizov, S.V., 1995. Colloids and Surfaces A: Physicochemical and Engineering Aspects 101, 1–7.
Nguyen, D.A., Fogler, H.S., Chavadej, S., 2001. Industrial & Engineering Chemistry Research 40, 5058–5065.
Patton, C.C., Casad, B.M., 1970. Society of Petroleum Engineers Journal 10, 17–24.
Remizov, S.V., Kirsanov, E.A., Matveenko, V.N., 2000. Colloids and Surfaces A: Physicochemical and Engineering Aspects 175, 271–275.
Ronningsen, H.P., 1992. Journal of Petroleum Science and Engineering 7, 177–213.
Russell, R.J., Chapman, E.D., 1971. Journal of the Institute of Petroleum 57, 117–128.
Sestak, J., Charles, M.E., Cawkwell, M.G., Houska, M., 1987. Journal of Pipelines 6, 15–24.
Singh, P., Fogler, H.S., Nagarajan, N.R., 1999. Journal of Rheology 43, 1437–1459.
Singh, P., Venkatesan, R., Fogler, H.S., Nagarajan, N.R., 2000. A.I.Ch.E. Journal 46, 1059–1074.
Singh, P., Youyen, A., Fogler, H.S., 2001a. A.I.Ch.E. Journal 47, 2111–2124.
Singh, P., Venkatesan, R., Fogler, H.S., Nagarajan, N.R., 2001b. A.I.Ch.E. Journal 47, 6–18.
Svendsen, J.A., 1993. A.I.Ch.E. Journal 39, 1377–1388.
Venkatesan, R., Singh, P., Fogler, H.S., 2002. SPE Journal 7, 349–352.
Viswanathan, T., Khilar, K.C., 1989. Canadian Journal of Chemical Engineering 67, 353–360.
Wardhaugh, L.T., Boger, D.V., 1991. A.I.Ch.E. Journal 37, 871–885.
Yi, Y.-B., Sastry, A.M., 2002. Physical Review E 66, 1–8.